LBL-10283
Preprint

Lawrence Berkeley Laboratory
UNIVERSITY OF CALIFORNIA

Submitted to the Journal of Physical Chemistry

RADIATION CHEMISTRY OF HEAVY PARTICLE TRACKS. II. THE FRICKE DOSIMETER SYSTEM

Aloke Chatterjee and John L. Magee

March 1980

Prepared for the U.S. Department of Energy under Contract W-7405-ENG-48

DISCLAIMER

RADIATION CHEMISTRY OF HEAVY PARTICLE TRACKS. II. THE FRICKE DOSIMETER SYSTEM

Aloke Chatterjee and John L. Magee

Biology and Medicine Division
Lawrence Berkeley Laboratory
University of California
Berkeley, CA 94720

Abstract

A heavy-particle track model suggested by considerations presented in a companion paper is used in a calculation of the differential (G') and integral (G) yields of the Fricke dosimeter system for six selected particles over a wide range of energies. The particles are H, He, C, Ne, Ar, and Fm; the energy range for the first two is 10^{-3} MeV/n to 10^{3} MeV/n, and for the last four is 10^{-1} MeV/n to 10^{3} MeV/n. The calculated G' and G values are compared with experimental values as far as possible, and the heavy-particle track model situation is discussed.

This work was supported by the U. S. Department of Energy under Contract W-7405-ENG-48.

The figures were printed from originals provided by the author.

1. Introduction

A companion paper[1] (hereafter called I) presents a general consideration of the radiation chemistry of heavy-particle tracks in aqueous systems, and suggests a heavy-particle track model. In this paper we report a calculation based on that model of the radiation chemical yields of the acidic ferrous sulfate system, commonly known as the "Fricke dosimeter."

The Fricke dosimeter[2,3] is the most studied of all aqueous systems, and its well understood characteristics have become a standard for comparison of yields under various conditions--both for experimental observations and for theoretical calculations. The system itself is 0.8N H_2SO_4, air saturated, and contains 10^{-3} M ferrous sulfate; sometimes a higher concentration, 10^{-2} M ferrous sulfate, is used, and then it is called the "super-Fricke dosimeter."

The decomposition products of water are of major importance for the radiation chemistry of any dilute aqueous solution. The radiation chemical decomposition of water in acid solution can be written as

$$H_2O \sim\!\!\!\sim\!\!\!\rightarrow H,\ OH,\ H_2,\ H_2O_2 \qquad (1)$$

In acid solution, all of the initially formed hydrated electrons are transformed into H atoms in less than 10^{-10} sec. The molecular products H_2, H_2O_2 and H_2O are formed in the "forward" reaction as the track expansion occurs.[4] The primary yields of the four products of eq 1 are G_H, G_{OH}, G_{H_2}, and $G_{H_2O_2}$, respectively,

which are the numbers of molecules formed per 100 eV of absorbed energy.

The aerated Fricke dosimeter has a G-value given by

$$G(Fe^{3+}) = 3G_H + G_{OH} + 2G_{H_2O_2} \tag{2}$$

based on the mechanism

$$H + O_2 \rightarrow HO_2 \tag{3}$$

$$Fe^{2+} + HO_2 \rightarrow Fe^{3+} + HO_2^- \tag{4}$$

$$HO_2^- + H^+ \rightarrow H_2O_2 \tag{5}$$

$$Fe^{2+} + OH \rightarrow Fe^{3+} + OH^- \tag{6}$$

$$2Fe^{2+} + H_2O_2 \rightarrow 2Fe^{3+} + 2OH^- \tag{7}$$

Attention in this calculation is focussed on the variation of yields arising from the patterns of energy deposited by heavy particles and simplifying assumptions are made whenever necessary to make the calculation feasible. We assume that 5.88 molecules of water are dissociated into H and OH for each 100 eV of absorbed energy (i.e., 17 eV is required per radical pair independent of the particle charge and energy). Other important approximations (e.g., prescribed diffusion), introduced in I are also used here. However, we use a

multiradical treatment whereas in ref. I all considerations are based on one-radical models.

The most important feature of this calculation is the separation of the deposited energy into two parts assigned to core and penumbra, respectively. Arguments for the validity of this concept for the case of a one-radical system are presented in I. The same simple arguments cannot be made for the more complex situation encountered in a multiradical system. A single radius of separation is difficult to define if there are several radicals with different diffusion constants and reaction rate constants. However, the concept of separation of a heavy particle track into core and penumbra is quite basic and we believe that it must apply in a multiradical system also. For the purpose of the present calculation we assume that a radius of separation can be introduced as an adjustable parameter. Once this parameter is obtained, the calculation is relatively straightforward.

The most elementary calculation of chemical yield is, of course, for $G'(Z;E)$ which is the differential yield[5] (i.e., the yield over a small segment of track) of a particle of atomic number Z and energy per nucleon, E. In order to get the ferric yield we must calculate G'_H, G'_{OH} and $G'_{H_2O_2}$ (see eq 2). Yields are considered separately in the core and penumbra regions. The total G' is then obtained by properly weighting the G''s of the core and penumbra according to the partitioning of the energy loss between them.

Once the differential yield is known as a function of energy per nucleon, the integral yields $G(Z;E)$ are obtained by means of the following relationship:

$$G(Z;E) = \frac{1}{E}\int_0^E G'(Z;E')dE' \qquad (8)$$

Calculations are reported for G'(Z;E) and G(Z;E) for the six representative particles over a wide range of energy.[6]

2. Methods of Calculation

The reactions of the Fricke system are given in Table I.[7] The primary radical recombination reactions shown under A in Table I gives the principal track effects and to a first approximation the reactions of A and C can be used to calculate the yields. It is generally assumed that some of the reactions of B are important for tracks in which high densities of radicals occur, and in our treatment, we use all of them.

The separation of core and penumbra is a valid approximation largely because the track reactions occur early. According to the discussion in I (Section 5) on the medium-LET case, after a short transient period the number of uncombined radicals in the expanding core remains constant. The fraction of initially formed radicals remaining uncombined decreases slowly as the expansion continues. The fraction of radicals surviving to react with the scavenger depends on r_1, but weakly. We use the separation parameter r_1 introduced in ref. I. In preliminary calculations other separations were used and the one which seems to give the best overall agreement with experimental results was chosen. The radii, r_1, in Figure 3 of I and the fraction of energy in the core, F_{core}, in Figure 4 of I apply to the calculation reported here. Values of LET_{core} are given by

$$LET_{core} = LET/2 + LET(1 + 2 \ln r_1/r_c)(4 \ln \sqrt{e}\, r_p/r_c)^{-1} \qquad (9)$$

where r_1 is the separation radius which is, of course, a function of Z and E; r_p and r_c are the penumbra and physical core radii, respectively (see Table I and Fig. 3 of I). For some particles at high energies $r_1 < r_c$; in these cases we take $r_1 = r_c$.

We use the concept, discussed in I, that radical-radical reactions dominate at first and scavenger reactions can be neglected. After a characteristic time given in the one-radical approximation by

$$t_1 = (k_s c_s)^{-1} \tag{10}$$

the scavenger reaction dominates. In a multiradical system such a time is actually difficult to define precisely and we choose $t_1 = 3\times10^{-7}$ sec for use in the calculations. If t_1 were determined by eq 10 of Table I with $c_{O_2} = 3 \times 10^{-4}$M, this value would be obtained. We prefer to think of t_1 as a parameter which can be adjusted.

The differential equations for the transient species and radiation products are shown in Table II. These equations include all of the reactions in A and B of Table I. The set of equations enclosed in the box include only the radical recombination reactions of A in Table I. An equation for the H_2O re-formed by radical combination must, of course, be included in this set (i.e., eq 2). The scavenger reactions of C (Table I) are not explicitly considered. It is, of course, assumed that they are dominant for times larger than t_1.

A. Applications of Spur-Model in the Core

A string of spurs is produced within the core, and each spur contains, on the average, 40 eV of energy. Thus, the average number of a given radical (H or OH) in a spur is equal to 40/17 at the onset of radical reactions. At low LET, spurs are formed separate from one another, and even when they expand because of the diffusion of their radicals, they remain isolated while the recombination reactions continue essentially to completion. Perhaps we should note that "completion" of the recombination reaction in a spur means that the maximum recombination has occurred, not that all radicals have recombined. We follow the expansion of the spur until $t = t_1$, the scavenger reaction time. At intermediate LET spurs are initially isolated from one another, but, as time progresses, they grow large enough so that radicals intermingle between neighboring spurs. Such a track core goes over to cylindrical expansion before the time $t = t_1$ is reached. At high LET, spurs overlap initially and the typical high-LET effects of radiation chemistry occur.

Table III gives a set of spur-expansion equations in the prescribed diffusion approximations for the limited set of reactions represented by the box in Table II. In our calculations we actually include all reactions under A and B in Table I. The complete set of differential equations actually used is not given in Table III because extension of the set shown to include all secondary reaction is trivial and can be done by inspection. Z_1, the inter-spur separation parameter, has been taken as $50/LET_{core}$ on the basis of the

agreement of calculation with experimental results. The average energy of a spur is 40 eV and so one might expect that Z_1 should be $40/LET_{core}$. Actually the consideration leading to the introduction of Z_1 involves several averages over distribution functions[1] and the situation is not so simple that the parameter can be chosen completely a priori.

The various r_j's which appear in the differential equations shown in Table III are parameters in our calculation associated with the initial distribution of radicals. In Table IV these initial radii for the various radical and molecular products are given along with the diffusion constants used. The radii for hydrogen and hydroxyl radicals are adjusted for very energetic protons in such a manner that the ferric yield in an isolated spur is 18.4.[8]

The system of differential equations of Table III (expanded to include all reactions A and B of Table I) are solved numerically from $t = 10^{-12}$ sec to 3×10^{-7} sec. These equations apply to a string of spurs but it is shown in ref. I that as the LET increases they go over into a form which is correct for a cylindrical distribution of radicals. We actually use the equations for all core calculations. The radicals of the penumbra which belong to the chemical core (i.e., in the region $r < r_1$), are included in the core as they become engulfed. At the cut-off time, $t = 3 \times 10^{-7}$ sec, the remaining H, OH, HO_2 and H_2O_2 react with Fe^{+2} to give the "calculated" Fe^{+3} yields of the core.

The discussion in ref. I of the core processes would tend to justify this procedure for the regions I and II. Region III, however, is one in which recombination dominates and in a strictly logical sense the model discussed in section 6 of the companion paper should be used, i.e., recombination should be calculated for non-diffusing radicals. Actually recombination is so fast and so nearly complete that both calculations give essentially the same results. For convenience the model used in regime I and II was continued into region III.

B. Penumbra Contribution

Calculation of the penumbra yield is discussed in I and the formula which applies is presented there (eq 37). The essential quantity needed in this calculation is $G_e(\varepsilon)$, the total Fe^{+3} yield of an electron of initial energy ε which is stopped in the Fricke system. A detailed consideration of the electron G-values is reported elsewhere.[8,9] In Table V we provide the parameters for empirically fitted formulas relating $G_e(\varepsilon)$ and ε in various energy intervals. When ε = 20 KeV or greater, the G-values for electrons can be represented by an analytical formula in a very convenient form which is also given in Table V.

3. Results

The results of the basic calculations of $G'_{core}(E)$ are presented in Figure 1. The calculational procedures strongly suggest that G'_{core} should be mainly a function of LET_{core} and a plot of G'_{core} vs LET_{core} (Figure 2) shows that a unique function is in fact obtained. The range of LET core values is very large (from 10^{-2} to 10^{3}eV/A) and the regions of the curve which apply to the individual particles are indicated. At low particle energies, where $F_{core} = 1$, the G'_{core} values of Figure 2 are expected to be the same as the total G'. At high particle energies, on the other hand, there is always a relatively large contribution from the penumbra and G'_{core} is significantly different from the total G'. The low-LET limit for G'_{core} is the same as G_{spur}, i.e., 18.4, whereas the total G' for the proton is around 15; under these conditions, the penumbra yield is lower than G'_{core} because of the track-end contributions to the latter.

In Figure 1, at all values of the abscissa the particles have the same velocity, and thus the same values of r_c and r_p. The penumbra contributions to G'(E), however, are not precisely the same because r_1 and F_{core} are different for particles with different Z. Figure 3 shows the G'_{pen} values for the six particles. The vertical arrows mark the energies for the various particles below which there is no penumbra (i.e., $F_{core} = 1$). $G'_{ko}(E)$ is the G-value for an ideal penumbra which contains all knock-on electrons from 100 eV to ϵ_{max}.

The differential G-value for a particle at energy per nucleon E is made up of a contribution from the core and a contribution from the penumbra as follows:

$$G'(E) = F_{core}(E)G'_{core}(E) + (1 - F_{core}(E))\, G'_{pen}(E) \qquad (13)$$

Using $F_{core}(E)$ values obtained from ref. I and the data of Figures 1 and 3, we calculate the G'(E) curves for the six particles shown in Figure 4. This figure summarizes the primary results of the calculations of this paper.

Figure 4 gives a broad view of the differential ferric yields for heavy particles. Some experimental data points are given for comparison with the calculations; at high energies, G'(E) can be measured directly. But at the lower energies, the data points are estimated from measured integral yields (i.e., G(E)). The directly measured values of Jayko et al.[10] for C, Ne and Ar are indicated by the dashed lines a, b and c, respectively. The experimental values are higher than the calculated curves by more than the estimated experimental error; it is known that nuclear fragmentation of the beam creates an error in the direction of increasing the yield, and part of the discrepancy lies here. A study of the effects of beam fragmentation by Christman et al.[11] is underway and the data will be re-evaluated.

Four sets of experimental data furnish estimates of the locations of the curve for H in the low energy region. The dashed curve d is an estimate by Schuler and Allen[12] of G'(E) from their experimental

data on G(E) for the deuteron; the open and closed circles are data points calculated from experimental G(E) values for the deuteron and proton, respectively, by Hart, Ramler and Rocklin;[13] the dashed curve e is an estimate of Pucheault and Julien[14] from experimental G(E) values for accelerated protons.

Two sets of experimental data furnish information on the location of the curve for He in the low energy region. The dashed curve f is the estimate by Schuler and Allen[12] of G'(E) based on an analysis of experimental G(E) for accelerated helium ions; the open squares are data points calculated from experimental G(E) values for α particles by Gordon and Hart.[15]

The calculation of G'(E) for H and He extended to E = 10^{-3} MeV/n is shown in Figure 5. The designation of experimental points is the same in Figure 5 as in Figure 4; another estimate of G'(E) by Collinson, Dainton and Kroh[16] based on G(E) values obtained from α particles is indicated by the dashed curve g. In the very lowest energy region the stopping power is not exclusively due to electronic excitation, and the values of the LET and the track structure are both uncertain.

The experimental data points in the low-energy region (E < 10 MeV/n) scatter so much that they do not furnish a real check on the model calculations. Although the model is rough and the qualitative aspects of track structure are not well known at low energies, calculated values are perhaps preferable to any particular set of experimental values because of an overall consistency in the former.

Figure 6 shows a plot of the G'(E) values of Figures 4 and 5 against LET. Although it has been widely assumed that heavy particle

tracks have yields which are simple functions of LET, the analysis presented in I makes it clear that this is not true. The curves for the various particles in Figure 6 are made up of two branches; the upper branch involves core and penumbra; at low energy below which only the core exists, all curves go to a lower branch identical with the curve of Figure 2 which is reproduced as the dashed curve.

The solid curves of Figures 7 and 8 give G(E) values calculated from the data of Figures 4 and 5 by means of eq 8. All of the experimental data points plotted for comparison are from direct measurements of G(E) values; data from which the estimates of G' values shown in Figures 4 and 5 were made are shown; in addition, G(E) values for accelerated protons by Kochanny et al.,[27] He nuclei by Anderson and Hart,[18] carbon by Schuler,[19] carbon and neon by Jayko et al.,[20] and data on fission fragments by Bibler are given.[21] Data obtained by Matsui et al.[22] for H and He are not indicated in the figures; they agree well with the H data of Hart et al.[13] and the He data of Anderson and Hart.[18]

The scatter of the experimental data points for G(E) is as large as that for G'(E). There is a suggestion, however, that G(E) rises more at low energies than our calculations show. Such a result could indicate that the track structure is significantly different from our model, perhaps because of nuclear collisions.

4. Discussion

The authors feel that the calculated curves presented in the figures give a good view of the Fricke dosimeter yields to be expected for accelerated heavy particles. As experimental values become better known, refinements may be made in the model so that calculations give agreement to any desired extent.

The calculation presented here assumes the G_{-H_2O} value for initial dissociation of water to be 5.88 and has three parameters which can be adjusted; they are r_1, Z_1 and t_1: All other parameters such as chemical reaction rate constants and diffusion constants were taken from known experimental values. The energy distribution in the penumbra is obtained from an a priori calculation. As the LET vs energy relationships for heavy particles and electrons become better known, this calculation may be improved. However, the radial energy distribution used is in satisfactory agreement with various experimental measurements and is probably one of the best known quantities. An a priori calculation of r_1 from the energy distribution requires several steps to get to the yield of radicals escaping from the electron tracks and then the use of an appropriate relationship such as $c_1 = k_s c_s / 2k$. We do not have a one radical system and we do not know how to do this. However, it is clear that the energy separation of the core and penumbra and thus the track G-values depend on the scavenger concentration. Accurate experimental heavy particle track yields as a function of c_s can perhaps be used to improve the heavy particle track model.

It is known that G-values of the Fricke dosimeter depend on ferrous concentration. For low-LET radiations, particularly electrons (in which we include γ-and X-rays) expressions for radical yields have a term linear in $c_s^{1/2}$,[23] and the ferric yield presumably varies in the same manner. It is a significant variation, but not a large one. A limited study of G-values of the Fricke dosimeter for heavy particle tracks as a function of ferrous concentration has been made,[22] but we have not attempted to explain these results in terms of the track model presented here.

The calculated G'-values are most reliable for the low LET particles (i.e., H and He at high energies) because these values are related in such a simple manner to the electron yields. For the same reason the low LET core calculations are reliable. The parameter Z_1 is introduced to take into account the overlapping of spurs along the core as LET increases. This parameter also allows for the overlapping with the penumbra which is engulfed and so it is not as simple as it appears at first. The high LET core calculation is independent of Z_1 and its reliability depends upon the validity of the separation (and non-interaction) of the core and penumbra. A discussion of this matter is presented in I.

There is a new interest in heavy particles which is concerned with high Z particles at high energies. Here the phenomena are not limited to radiation chemical effects but also with physical and biological effects. High-energy, heavy nuclei can interact with the nuclei of the medium in several ways. One of the most important types of

nuclear interactions is the production of lighter fragments of the incident particle which dilutes the main beam with lower atomic number fragments. In addition to the projectile fragmentation, target fragmentation is also possible. The projectile fragments emerge from the interaction site in a direction very close to that of the incoming primary heavy ion, and with little or no change in velocity from that of the primary. Target fragments are characterized by a broad angular distribution, relatively low energies, and high multiplicity. At present, our understanding of nuclear fragmentation characteristics is rather qualitative. Knowledge of the cross-sections for production of these fragments are neither available from experimental measurements nor is it possible to calculate them theoretically with any confidence. Hence, we have not been able to introduce in our calculation the chemical effects of the nuclear secondaries. We know, however, that the introduction of low Z fragments in the beam can change the radiation chemical yields substantially. In Figure 4, when we compare our theoretical results with the experimental measurements of Jayko et al.,[10] we find that the discrepancies are in the right direction. For example, curve a, which is a result of the measurements made with carbon beam, lies above the "theoretical" result for a pure beam. We believe that this is a result of nuclear fragmentation. The lower atomic number nuclear secondaries increase the ferric yield, and thus effectively giving higher values than for a virgin carbon beam. Similar explanation may hold true for curves b (for neon) and c (for argon). Cross-section measurements are in progress

in our laboratory, and once they become available, incorporation of their effects in our calculation procedures will be a straightforward matter. In the meantime a study of the fragmentation problem with theoretical estimates of the cross sections is being made by Christman et al.[11] and their results should be available in the near future.

In summary, calculations of G'- and G-values of the Fricke dosimeter system are presented to illustrate the use of a heavy-particle track model described in a companion paper. The curves shown in the figures give a good overall view of the yields, and we do not expect the patterns to change substantially as better experimental data for particle irradiations become available. The calculation itself can be refined in many ways, but we believe that the principal track phenomena are included.

References

1. J. L. Magee and A. Chatterjee, this journal, preceding paper. We call this ref. I.

2. H. Fricke and E. J. Hart in "Radiation Dosimetry," vol. 2, F. H. Attix and W. C. Roesch, eds., Academic Press, New York, N. Y., 1976, p. 107.

3. G. G. Jayson, B. J. Parsons and A. J. Swallow, Int. J. Radiat. Phys. Chem. 7, 363 (1975).

4. The recombination of H and OH radicals must lead to a certain amount of H_2O re-formation. In the radiolysis of water this reaction is not actually observable, but it is always included in the reaction schemes (see Table I).

5. See ref. I for a discussion of differential (G') and integral (G) yields, their relationship to each other, specification of arguments, etc.

6. The six particles are H, He, C, Ne, Ar, and Fm. The first two (H, He), the lightest of the "heavy" particles, have been widely used in accelerators; the next three (C, Ne, Ar) are the principal heavy particles currently accelerated in the BEVALAC; the last (Fm) has atomic number 100, and is representative of the very heaviest particles. The energy range for the first two (H, He) is 10^{-3} MeV/n $\leq$ E $\leq$ 10^{3} MeV/n; for the last four (C, Ne, Ar, Fm) it is 10^{-1} MeV/n $\leq$ E $\leq$ 10^{3} MeV/n.

7. This is a simplified set of equations which is usually given for the system. A more complete discussion of the mechanism is given in ref. 3.

8. J. L. Magee and A. Chatterjee, J. Phys. Chem. 82, 2219 (1978).

9. In ref. 8, $G_e(\varepsilon)$ values were obtained with a model using $t_1 = 3 \times 10^{-6}$. The dependence of the yields of low LET radiations on the concentration of scavengers (and hence on effective t_1 values) is so small that we use the previous results instead of recalculating $G_e(\varepsilon)$ to be consistent with the $t_1 = 3 \times 10^{-7}$ used in this paper.

10. M. Jayko, A. Appleby, E. Christman, A. Chattejee and J. L. Magee, Lawrence Berkeley Laboratory Report LBL-7432, University of California, Berkeley 1978.

11. E. A. Christman, A. Appleby and M. Jayko, forthcoming.

12. R. H. Schuler and A. O. Allen, J. Am. Chem. Soc. 79, 1565 (1957).

13. E. J. Hart, W. J. Ramler, and S. R. Rocklin, Radiat. Res. 4, 378 (1956).

14. J. Pucheault and R. Julien, "Proceedings of the Third Tihany Symposium on Radiation Chemistry," J. Dobo and P. Hedwig, eds., Vol. 2, 1972, p. 1191.

15. S. Gordon and E. J. Hart, Radiat. Res. 15, 440 (1961).

16 E. Collinson, F. S. Dainton and J. Kroh, Proc. Roy. Soc., London, 265A, 407 (1962).

17. G. L. Kochanny, Jr., A. Timnick, C. J. Hochanadel, and C. D. Goodman, Radiat. Res. 19, 462 (1963).

18. A. R. Anderson and E. J. Hart, Radiat. Res. 14, 689 (1961).

19. R. H. Schuler, J. Phys. Chem. 71, 3712 (1967).

20. M. E. Jayko, T-L. Tung, G. P. Welch, and W. M. Garrison, Biochem. and Biophys. Res. Comm. 68, 307 (1976).

21. N. E. Bibler, J. Phys. Chem. 79, 1991 (1975).

22. M. Matsui, H. Seki, T. Karasawa and M. Imamura, J. Nucl. Sci. and Tech. 7, 97 (1970).

23. This concentration variation has not actually been verified for the Fricke dosimeter system; for another aqueous system see T. Balkas, J. H. Fendler and R. H. Schuler, J. Phys. Chem. 74, 4497 (1970); see also A. Mozumder and J. L. Magee, Int. J. Radiat. Phys. and Chem. 7, 83 (1975).

24. These reaction rate constants are chosen from tables published by the National Bureau of Standards. (A) M. Anbar, Farhataziz and A. B. Ross, NSRDS-NBS 51 (1975). (B) Farhataziz and A. B. Ross, NSRDS-NBS 59 (1977).

Table I. Reactions in the Fricke system

Reactions	Reaction Rate Constant (liters/mole sec)
A. Recombination of Primary Radicals	
1. $H + H \rightarrow H_2$	1×10^{10}
2. $H + OH \rightarrow H_2O$	2.4×10^{10}
3. $OH + OH \rightarrow H_2O_2$	4×10^{9}
B. Reactions of Radicals and Product Molecules	
4. $H + H_2O_2 \rightarrow H_2O + OH$	1×10^{8}
5. $OH + H_2O_2 \rightarrow H_2O + HO_2$	5×10^{7}
6. $OH + H_2 \rightarrow H_2O + H$	6×10^{7}
7. $HO_2 + H \rightarrow H_2O_2$	1×10^{10}
8. $HO_2 + OH \rightarrow H_2O + O_2$	1×10^{10}
9. $HO_2 + HO_2 \rightarrow H_2O_2 + O_2$	2×10^{6}
C. Scavenger Reactions	
10. $H + O_2 \rightarrow HO_2$	1×10^{10}
11. $HO_2 + Fe^{+2} \rightarrow HO_2^- + Fe^{+3}$	2×10^{6}
12. $OH + Fe^{+2} \rightarrow OH^- + Fe^{+3}$	3×10^{8}
13. $H_2O_2 + Fe^{+2} \rightarrow OH^- + OH + Fe^{+3}$	56

Table II. Differential equations for transient species and radiation products in track.

$$\frac{d}{dt}(H) = -2k_1(H)^2 - k_2(H)(OH) - k_4(H)(H_2O_2) + k_6(OH)(H_2) - k_7(HO_2)(H)$$

$$\frac{d}{dt}(OH) = -k_2(H)(OH) - 2k_3(OH)^2 + k_4(H)(H_2O_2) - k_5(OH)(H_2O_2) - k_6(OH)(H_2) - k_8(HO_2)(OH)$$

$$\frac{d}{dt}(H_2O) = k_2(H)(OH) + k_4(H)(H_2O_2) + k_5(OH)(H_2O_2) + k_6(OH)(H_2) + k_8(HO_2(OH)$$

$$\frac{d}{dt}(H_2) = k_1(H)^2 - k_6(OH)(H_2)$$

$$\frac{d}{dt}(H_2O_2) = k_3(OH)^2 - k_4(H)(H_2O_2) - k_5(OH)(H_2O_2) + k_7(HO_2)(H) + k_9(HO_2)^2$$

$$\frac{d}{dt}(HO_2) = k_5(OH)(H_2O_2) - k_7(HO_2)(H) - k_8(HO_2)(OH) - 2k_9(HO_2)^2$$

$$\frac{d}{dt}(O_2) = k_8(HO_2)(OH) + k_9(HO_2)^2$$

Table III. Track equations in prescribed diffusion.

$$\frac{d\nu_1}{dt} = -\frac{2k_1\nu_1^2}{[2\pi(r_1^2 + 4D_1t)]^{3/2}}\left[1 + \frac{[2\pi(r_1^2 + 4D_1t)]^{1/2}}{Z_1}\right]$$

$$-\frac{k_2\nu_1\nu_2}{[\pi(r_1^2 + r_2^2 + 4D_1t + 4D_2t)]^{3/2}}\left[1 + \frac{[2\pi(r_1^2 + r_2^2 + 4D_1t+4D_2t)]^{1/2}}{Z_1}\right]$$

$$\frac{d\nu_2}{dt} = -\frac{k_2\nu_1\nu_2}{[\pi(r_1^2 + r_2^2 + 4D_1t + 4D_2t)]^{3/2}}\left[1 + \frac{[\pi(r_1^2 + r_2^2 + 4D_1t + 4D_2t)]^{1/2}}{Z_1}\right]$$

$$-\frac{2k_3\nu_2^2}{[2\pi(r_2^2 + 4D_2t)]^{3/2}}\left[1 + \frac{[2\pi(r_2^2 + 4D_2t)]^{1/2}}{Z_1}\right]$$

$$\frac{d\nu_3}{dt} = \frac{k_2\nu_1\nu_2}{[\pi(r_1^2 + r_2^2 + 4D_1t + 4D_2t)^{3/2}}\left[1 + \frac{[2\pi(r_2^2 + 4D_2t)]^{1/2}}{Z_1}\right]$$

$$\frac{d\nu_4}{dt} = \frac{k_1\nu_1^2}{[2\pi(r_1^2 + 4D_1t]^{1/2}}\left[1 + \frac{[2\pi(r_1^2 + 4D_1t)]^{1/2}}{Z_1}\right]$$

$$\frac{d\nu_5}{dt} = \frac{k_3\nu_2^2}{[2\pi(r_2^2 + 4D_2t)]^{3/2}}\left[1 + \frac{[2\pi(r_2^2 + 4D_2t)]^{1/2}}{Z_1}\right]$$

Table IV. Values of initial radii and diffusion constants

Species	Initial Radius (A)	Diffusion Constant (cm^2/sec)
H	26	$8x10^{-5}$
OH	13	$2x10^{-5}$
H_2	26	$8x10^{-5}$
HO_2	26	$2x10^{-5}$
H_2O_2	13	$2x10^{-5}$
O_2	26	$2x10^{-5}$

Table V. Relationship between $G_e(\varepsilon)$ for ferric yield and electron energy ε at various energy intervals

I. For $\varepsilon \leq 20$ keV,

$$G_e(\varepsilon) = a_0 + a_1 \ln(\varepsilon) + a_2 [\ln(\varepsilon)]^2$$

Energy Interval	a_0	a_1	a_2
100 eV - 500 eV	71.1	-19.7	1.52
500 eV - 1000 eV	42.3	-10.2	0.746
1000 eV - 1600 eV	17.6	-3.07	0.225
1600 eV - 3200 eV	-168	40.2	-2.23
3200 eV - 5000 eV	-102	23.9	-1.22
5000 eV - 10000eV	10.3	-0.366	0.079
10000 eV - 20000 eV	6.04	0.878	-0.006

II. For $\varepsilon > 20$ keV

$$G_e(\eta) = 18.4 - \frac{9.7337}{\eta 0.6} F(\eta)$$

where $\eta = \ln(\varepsilon/200)$ and $F(\eta) = 1 + \frac{0.1936}{\eta} + \frac{0.1587}{\eta^2} + \frac{0.2752}{\eta^3}$

Figure Legends

1. Calculated differential core yields, $G'_{core}(E)$, for the six representative particles vs. the energy per nucleon, E.
2. Calculated differential core yield, $G'_{core}(LET_{core})$ vs. (LET_{core}).
3. Calculated penumbra yields, $G'_{pen}(E)$, for the six representative particles vs. the energy per nucleon, E. The vertical arrows mark the energy limits below which no penumbra exists. The curve marked $G'_{ko}(E)$ gives the yield of the complete spectrum of knock-on electrons from 100 eV to ϵ_{max} corresponding to the energy E.
4. Calculated differential yields G'(E), for the six representative particles vs. energy per nucleon, E, are given by the solid curves. Estimates of values for C, Ne and Ar from direct experimental measurements by Appleby et al. are indicated by the dashed lines a, b, and c, respectively. In the low energy region (below 10 MeV/n, estimates have been made from analysis of integral G-values by various authors. For H: ●, Hart, Ramler and Rocklin; dashed curve e, Pucheault and Julien. For D: o, Hart, Ramler and Rocklin; dashed curve d, Schuler and Allen. For He: □, Gordon and Hart; dashed curve f, Schuler and Allen.
5. Calculated differential yields, G'(E), for H and He in the low-energy region are given by the solid curves. Estimates of various authors based on analysis of their experimental results on integral G-values are shown. For H: ●, Hart, Ramler and Rocklin;

dashed curve e, Pucheault and Julien. For D: o, Hart, Ramler and Rocklin; dashed curve d, Schuler and Allen. For He: □, Gordon and Hart; dashed curve f, Schuler and Allen; dashed curve g, Collison, Dainton and Kroh.

6. Calculated differential yields, G'(E), for the six representative particles vs. total LET are given by the solid curves. The calculations for C, Ne, Ar, and Fm are in the range $0.1 \leq E \leq 100$; the calculation for H and He are in the range of $0.001 \leq E \leq 100$. The dashed curve indicates the common curve which is obtained under conditions in which the penumbra vanishes.

7. Calculated integral yields, G(E), for the six representative particles vs. the energy per nucleon, E, are given by the solid curves. Experimental measurements of various authors are indicated by the plotted points; dashed durves give some of the authors' estimates of best curves drawn through their data points. For H: ●, Hart, Ramler and Rocklin; ▲, Anderson and Hart; x, Kochanny, et al.; dashed curve b, Pucheault and Julien. For D: o, Hart, Ramler and Rocklin; △, Anderson and Hart; dashed curve a, Schuler and Allen. For He: ■, Anderson and Hart; □ Gordon and Hart; dashed curve c, Schuler and Allen. For C: ▽, Schuler; ▼, Jayko et al. For Ne: J, Jayko, et al. For fission fragments: F, Bibler.

8. Calculated integral yields, G(E), for H and He in the low-energy region are given by the solid curves. Various experimental results are also shown. For H: o, Hart, Ramler and Rocklin; dashed curve b, Pucheault and Julien. For D: o, Hart; dashed curve b, Pucheault and Julien. For D: ●, Hart, Ramler and Rocklin; ▲, Anderson and Hart; dashed curve a, Schuler and Allen. For He: ■, Anderson and Hart; □, Gordon and Hart; ϕ, Collinson, Dainton and Kroh; dashed curve c, Schuler and Allen.

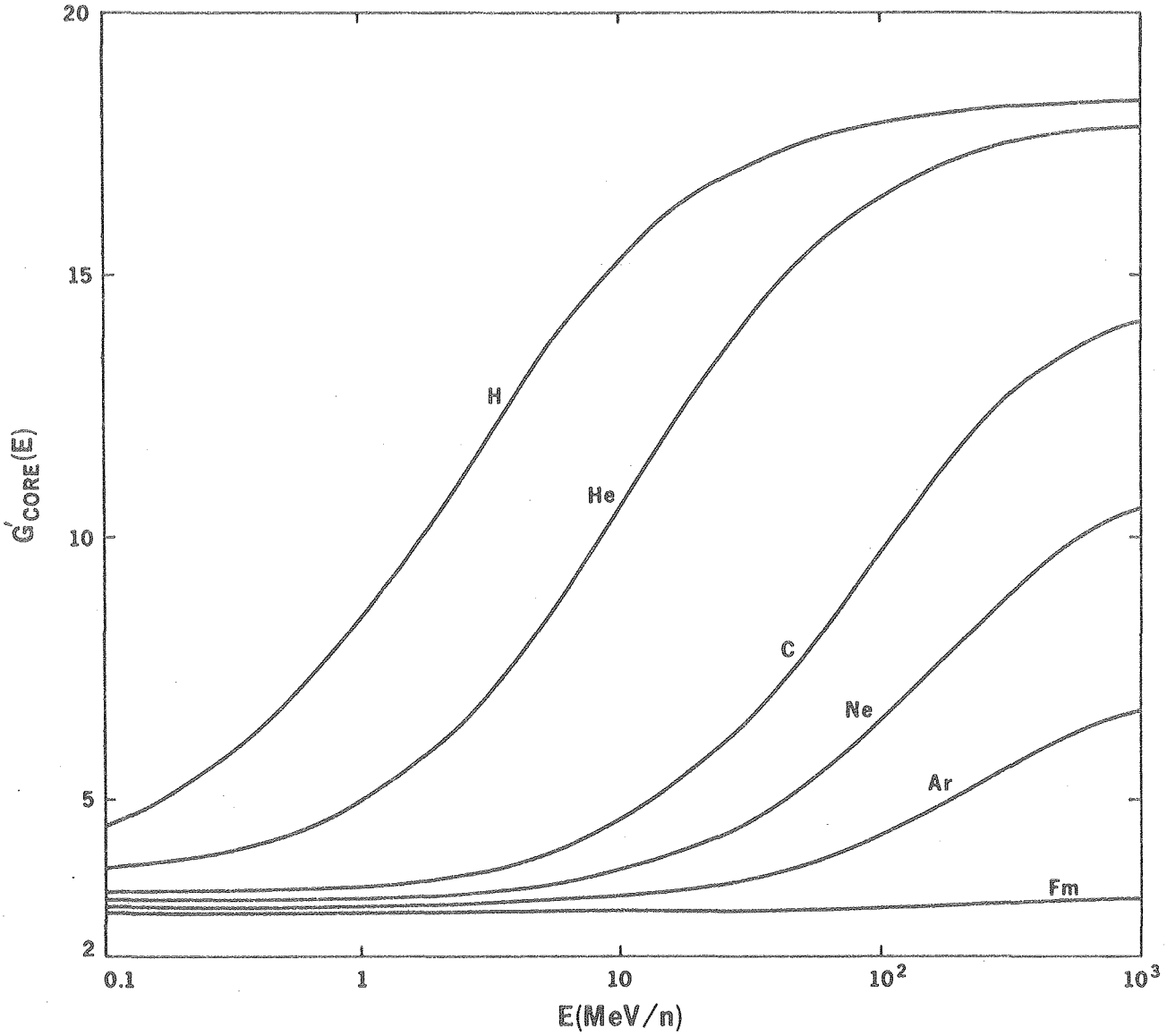
20
15
10
5
2
$G'_{CORE}(E)$
H
He
C
Ne
Ar
Fm
0.1
1
10
10^2
10^3
E(MeV/n)
XBL 803-8503

Fig. 1

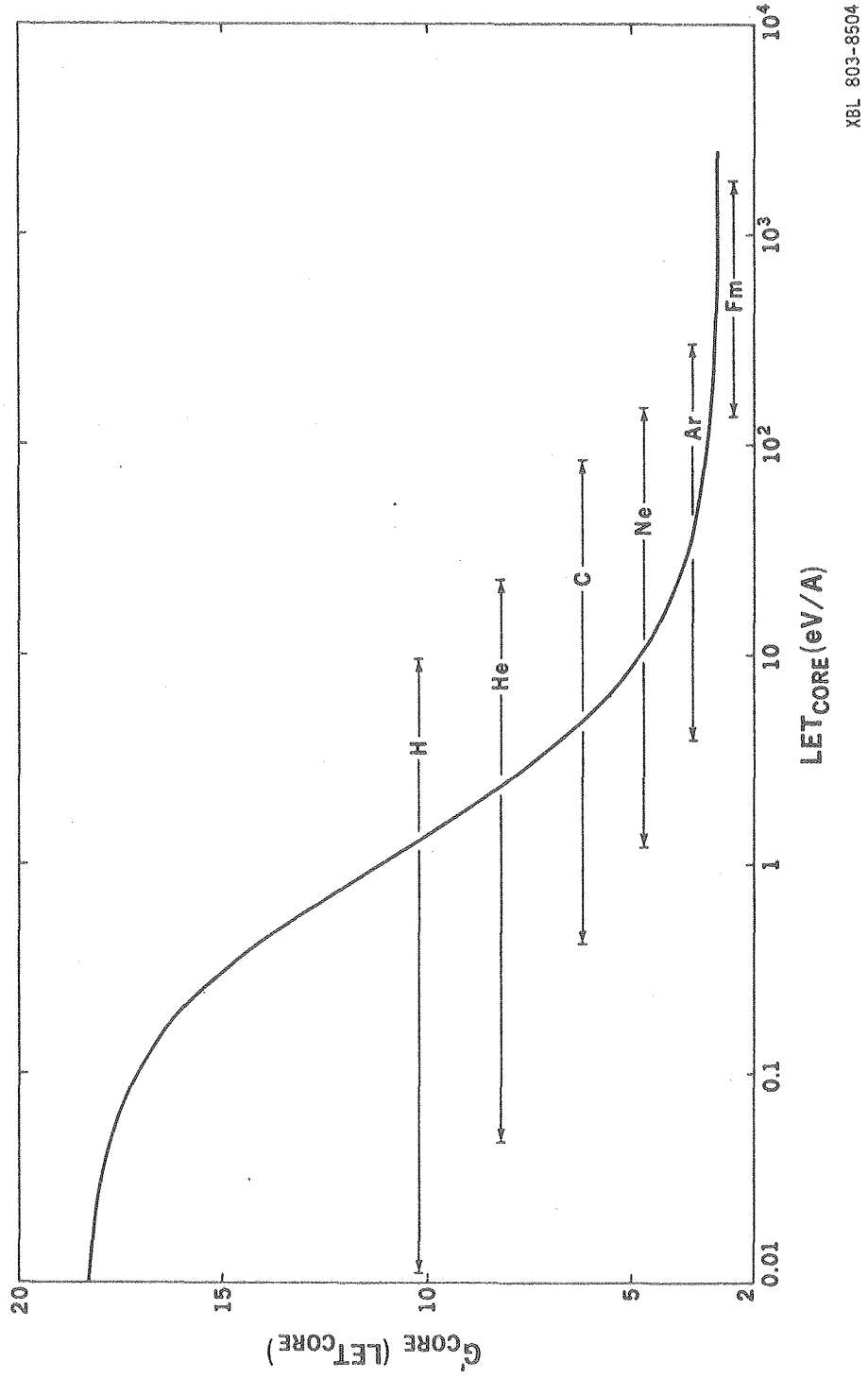
G_{CORE} (LET_{CORE})
20
15
10
5
2
0.01
0.1
1
10
10^2
10^3
10^4
LET_{CORE}(eV/A)
H
He
C
Ne
Ar
Fm
XBL 803-8504

Fig. 2

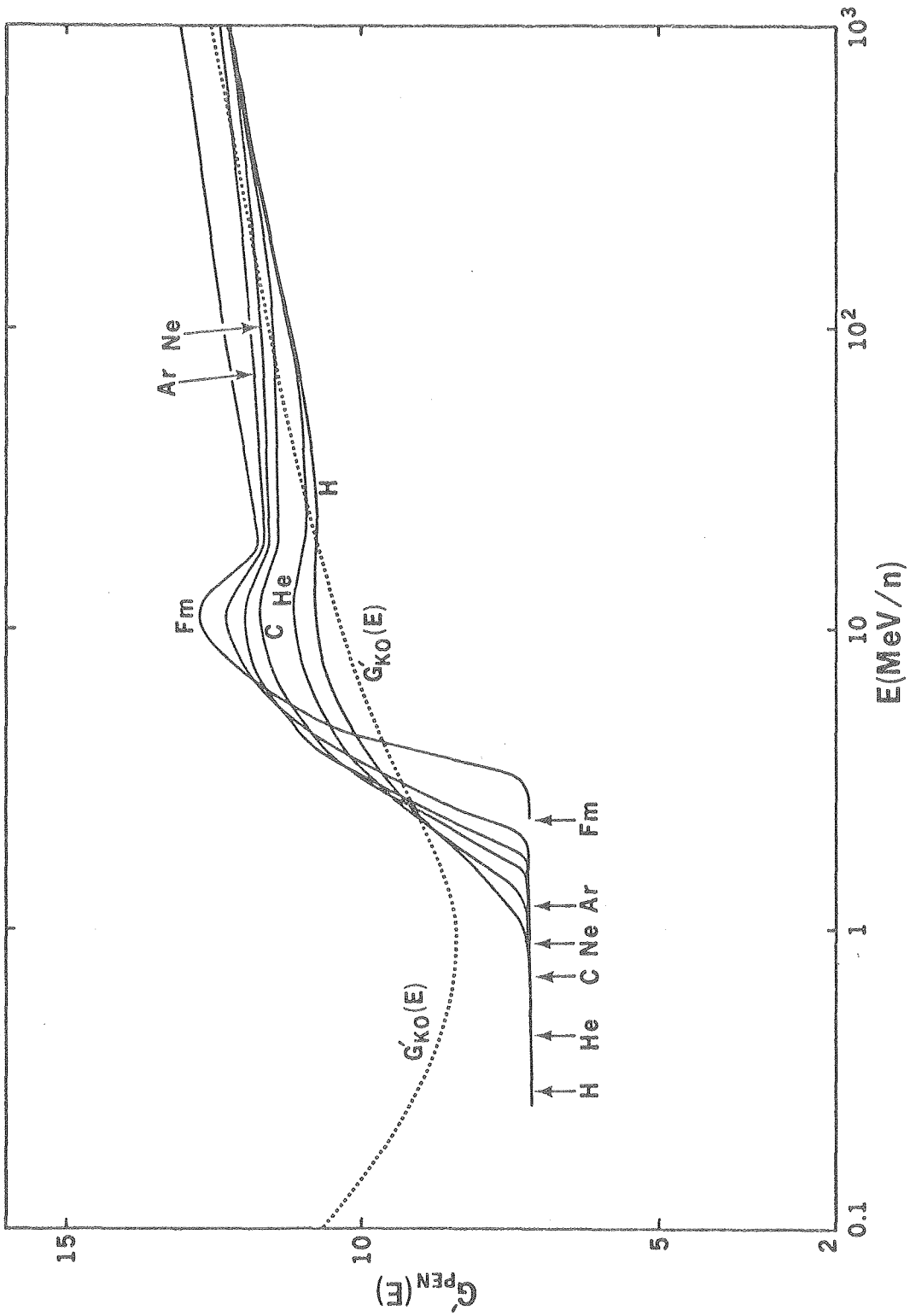

XBL 7911-12797

Fig. 3

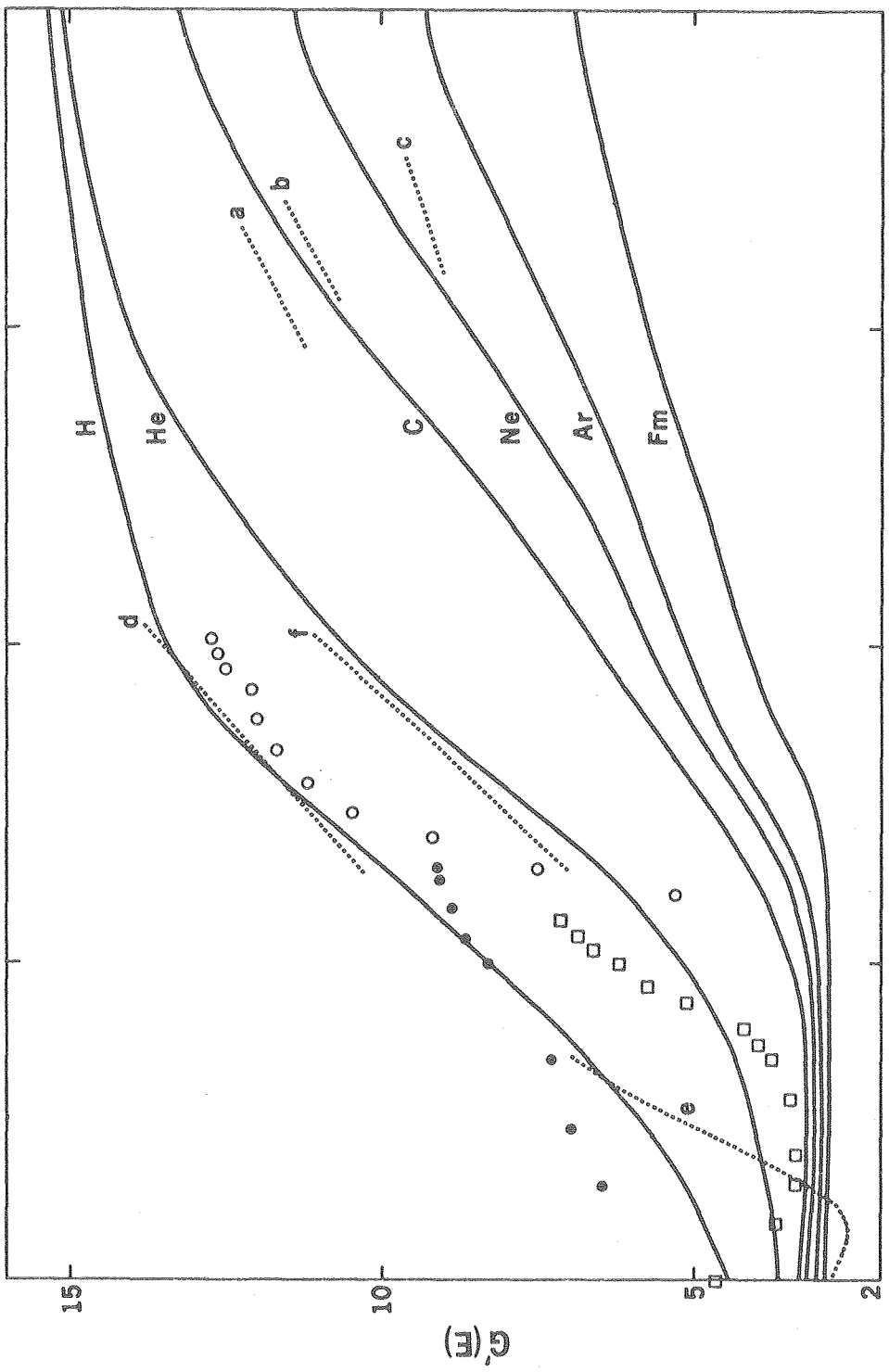

XBL 803-8508

Fig. 4

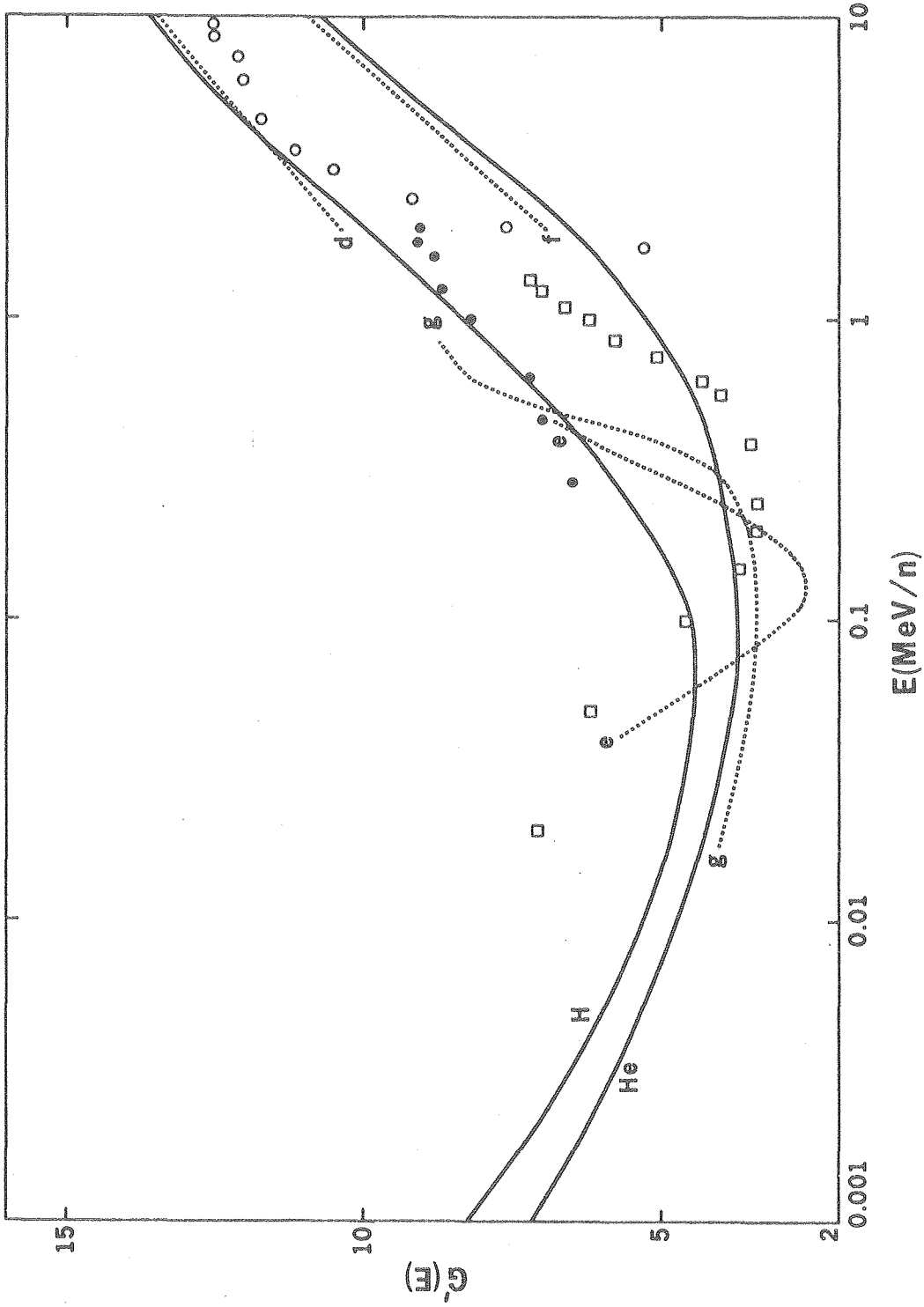

XBL 803-8509

Fig. 5

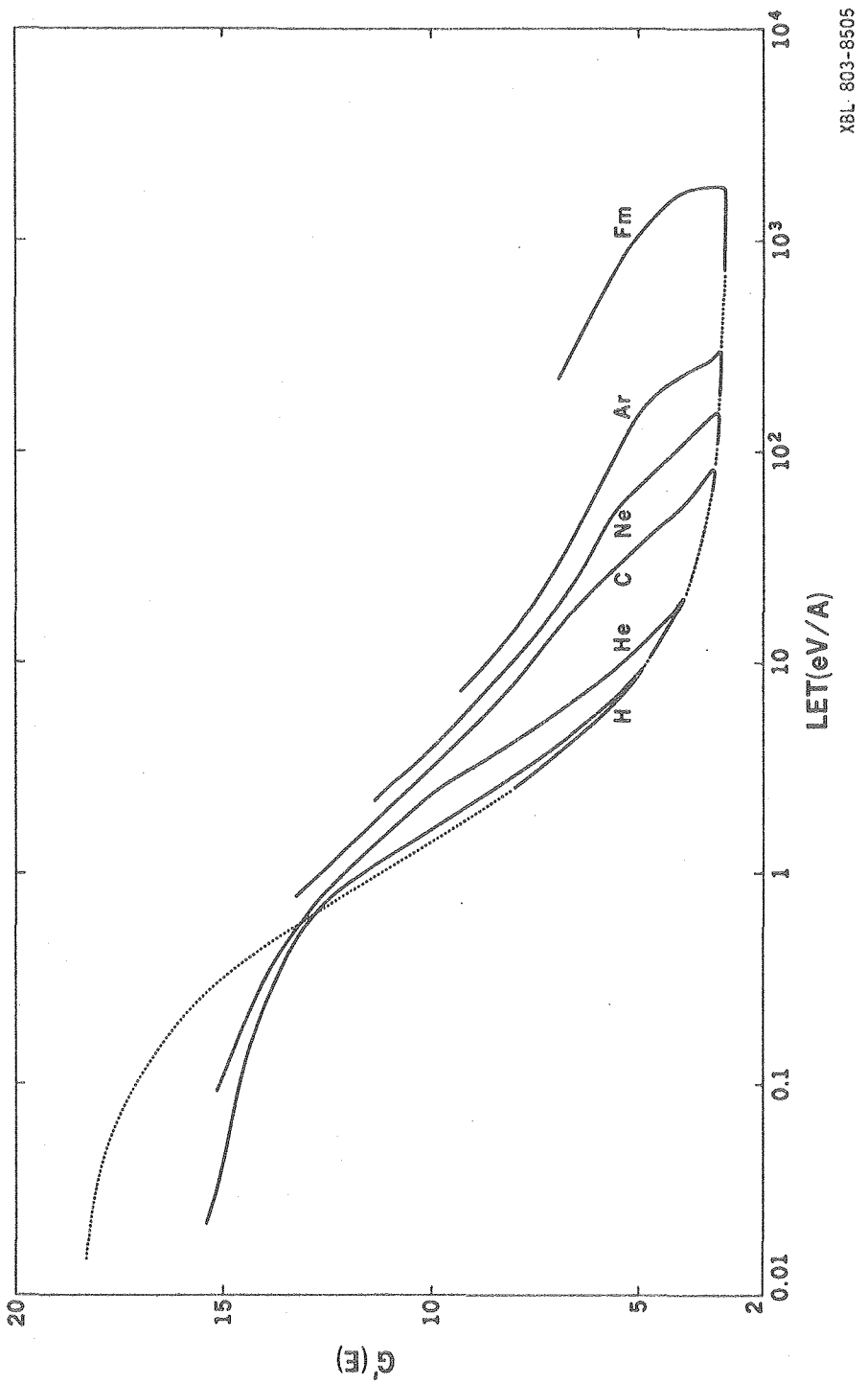
G'(E)
20
15
10
5
2
0.01
0.1
1
10
10^2
10^3
10^4
LET(eV/A)
H
He
C
Ne
Ar
Fm
XBL 803-8505

Fig. 6

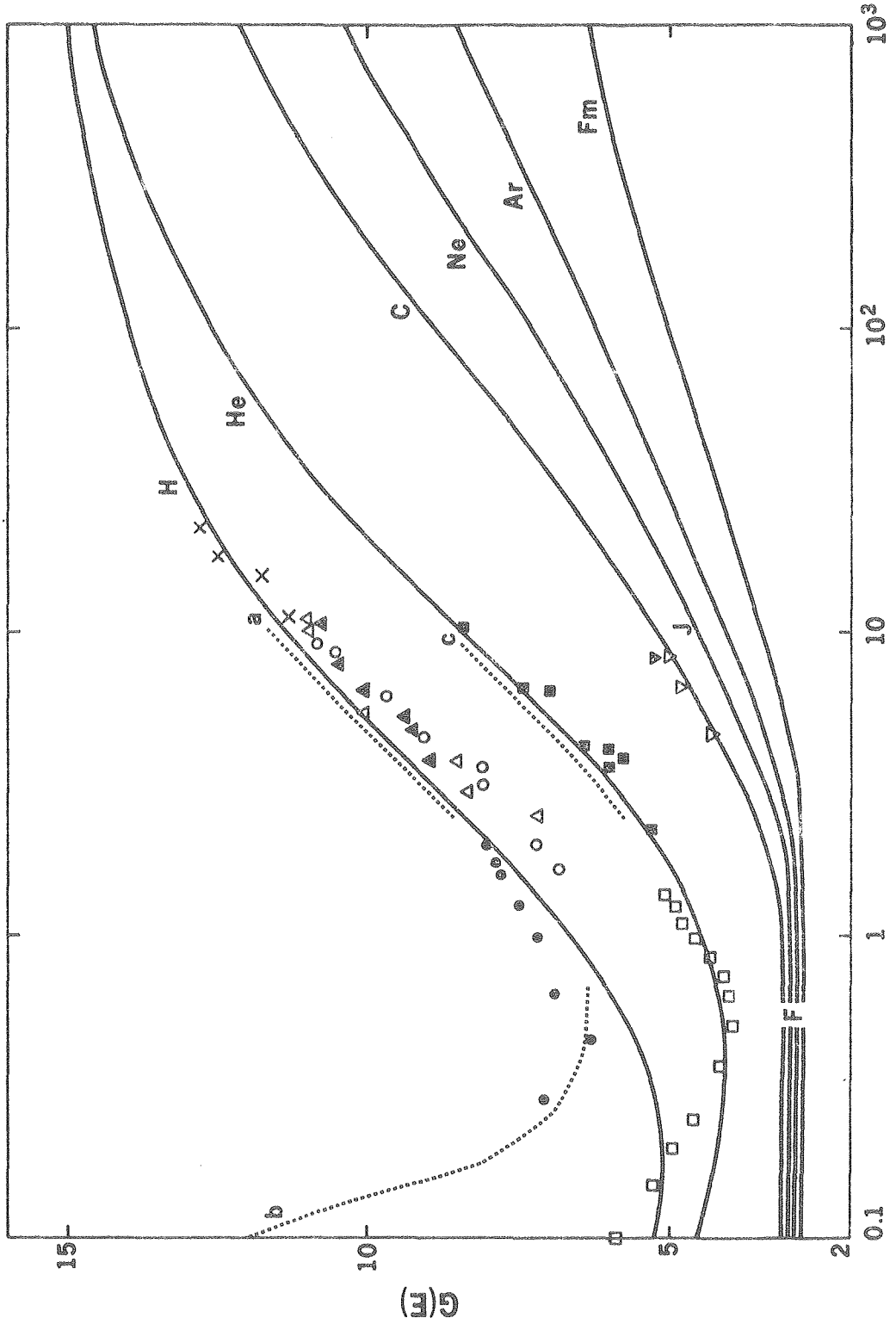

XBL 803-8506

Fig. 7

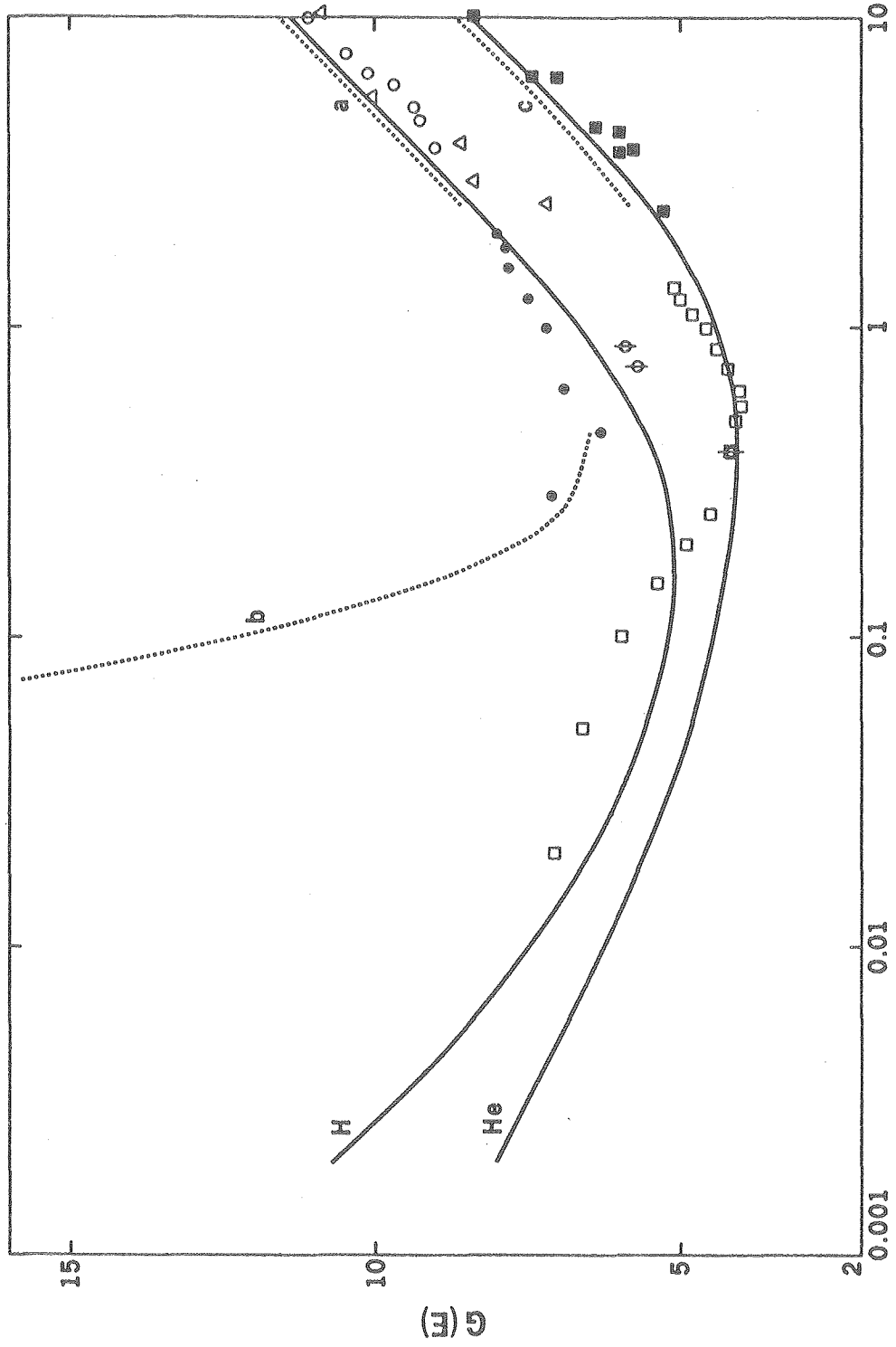

XBL 803-8507

Fig. 8